Mol Cell Toxicol (2012) 8:217-227
DOI 10.1007/s13273-012-0027-3

ORIGINAL PAPER

# Cytotoxicity of core-shell polystyrene magnetic beads and related mechanisms

**Li Li Wang[1], Kun Zhang[1], Chun Yang Xiong[1,2] & Zi Gang Ge[1,2]**

Received: 9 May 2011 / Accepted: 25 November 2011


**Abstract** Magnetic particles (MPs) of nano/submicron-scale have been widely used in biomedical applications and laboratory research. It is vital to evaluate the performance and influence of MPs incubated with cells. This study aimed to test the cytotoxicity of core-shell polystyrene magnetic beads and explore the related mechanisms for further use in cartilage regeneration. Core-shell polystyrene magnetic beads at 0-2 ng/cell were incubated with human chondrocyte cell line C28/I2 for five days. Cell viability, proliferation, morphology and expression of key genes that regulate the cell function were evaluated. The results were compromised in a dose- and time-dependent way. There were visible cytotoxic effects at a high loaded dose of 2 ng/cell, such as cell uptake, low viability, slow proliferation rate and poor cell morphology. Gene expression was a balanced consequence between toxic factors and cell repair performances. Core-shell polystyrene magnetic beads showed acceptable biocompatibility except at higher doses (over 2 ng/cell) where low cytotoxicity was apparent. These interferences were probably owing to ROS (reactive oxygen species) generation, cytoskeleton architecture rearrangement, iron imbalance, modification detachment, etc.

**Keywords** Core-shell, Magnetic beads, Biocompatibility, Mechanism

[1]Department of Biomedical Engineering, College of Engineering, Peking University, Beijing 100871, P.R. China
[2]Center for Biomaterials and Tissue Engineering, Academy for Advanced Interdisciplinary Studies, Peking University, Beijing 100871, China
Correspondence and requests for materials should be addressed to Z. G. Ge (✉ gez@pku.edu.cn)

In recent years, magnetic particles (MPs) of nano/submicron-scale have been widely utilized in biomedical research[1], including in hyperthermia, high throughput screening, labeling and tracking, Magnetic resonance imaging (MRI) and Magnetic force microscopy (MFM), drug delivery, etc[2,3]. Endowed with unique magnetic properties and easily fabricated, MPs have become promising candidates for biomedicine, biomechanics, biotechnology and cell biology[2,3]. For clinical trials, MPs in the nanos-cale order have been adopted to label, track, and image cells efficiently[4]. Additionally, MPs are capable of inducing tumor degeneration through heated effects[5]. For research practices, proper magnetic forces can be applied to trigger physical stimuli for promoting a biomimetic environment, inducing cell differentiation and improving cell functionality[6]. MPs are also used in techniques for manipulating and analyzing bioactive arrays, which are crucial to biochip development and flow cytometry screening[7,8]. For *in vitro* and particularly *in vivo* applications, the biocompatibility of MPs has attracted further attention.

Most MPs scale from nanometers to micrometers, and their structures can be grouped into one of the three categories: free particles, core-shell form, or embedded type[9,10]. A core-shell unit has an inorganic or organic core wrapped with numbers of magnetic metal oxide and coated with a biocompatible surface outside, for instance carboxyl or amino groups, dextran, albumin, polyethylene glycolide (PEG), etc[3]. Core-shell MPs are the most broadly used type for their low toxic and easily fabricated properties. Embedded MPs are fabricated by integrating polymers, hydrogels or amphiphilic molecules with magnetic metal oxide with an aim to increase size, stability and biocompatibility[9,11,12]. These two strategies can prevent the agglomeration of free particles and reduce direct contact between iron and bioactive substances[13].

The biocompatibility of MPs depends on multiple parameters, including the fabrication process, shape, size, surface modification and specific cell type[3]. Ferrous or ferric oxide is the main functional component usually. Though most studies showed that coating or embedding could improve biocompatibility of MPs[14], some others argued that these improvements were not obvious[15]. MPs of bead-shape showed lower toxicity than any other shape (rod, worm and sphere)[16]. Negative COOH-modified MPs performed better biocompatibility than positive $NH_2$- or none modificatied ones[17,18]. Apparent disparities could be observed among various cell lines even with MPs of the same size, composition and modification[19,20]. Additionally, pronounced toxicity was only observed over 100 μg/mL, while low or no cytotoxicity was found below, indicating a dose-dependant way[2]. Thus, it is essential to investigate the cytotoxicity of the core-shell polystyrene magnetic beads and found safe dosage to the human chondrocytes for further applications in cartilage regenerative study.

It is widely agreed that MPs can compromise cells and tissues through three possible mechanisms. First, the uptake and accumulation of insoluble particles and their subsequent interaction with bioactive molecules like medium or cellular components lead to cellular stress and even necrosis[21]. Small MPs, especially smaller than 100 nm[22], can gather in the cytoplasm around the nucleus through either endocytosis or passive diffusion[6,23]. Second, the induced oxidative stress which causes DNA damage, mitochondrial impairment, phospholipids lesion and protein injury[24] can lead to cytotoxicity and apoptosis. Thirdly, the ferrous or ferric iron may harm cells through altering pH, ionic homeostasis, electric potential and protein function[2,3]. To sum up, exposure to MPs can incur significant toxic effects, such as inflammation, apoptotic bodies formation, impaired mitochondrial function, chromosome condensation and DNA damage[25,26].

Though the biocompatibility of MPs has been extensively investigated, some questions remain unexplored. Different units have been used to characterize the concentration of MPs, such as μg/mL, mM and pg/cell, which makes the interpretation of results difficult. In this study, a comprehensive *in vitro* experiment was conducted to investigate the cytotoxicity of core-shell magnetic beads of 100-500 nm with human chondrocyte cell line C28/I2 and to find the proper dosage for further researches in cartilage regeneration. C28/I2 is reported to be closest to primary chondrocytes with respect to functional gene expression among the immortalized human chondrocyte cell lines[27]. Cell viability, proliferation, morphology, adhesion, and molecular biocompatibility with sequential MPs/cell ratios

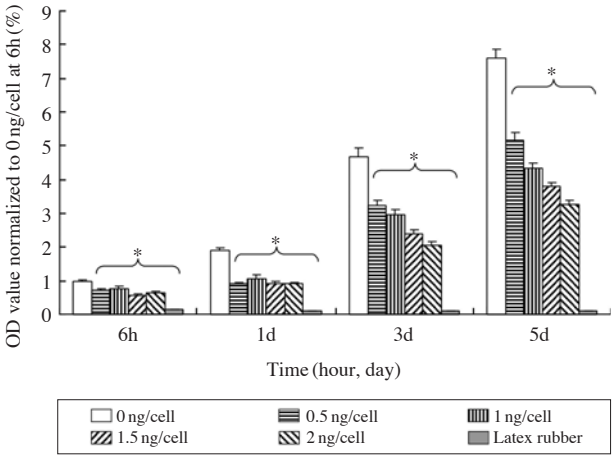


**Figure 1.** MTT assay result used to investigate the cytotoxicity of incubation with magnetic beads. 0-2 ng/cell groups were tested at 6h, 1d, 3d and 5d. OD value was normalized according to the negative control (0 ng/cell) (%), at 6h and the latex rubber cut into 0.5∗0.5 cm as the positive control. There was a visible dose- and time-dependent reduction of cell viability between other groups and the negative control. At early stage, the data among different experimental groups (0.5-2 ng/cell) were similar to each other. As time progressed, especially after 3d, higher concentration group showed lower cell viability. A significant difference at the same time point of each investigated group (0.5-2 ng/cell, latex rubber) to the negative control was denoted with asterisk ($P < 0.05$, n=5).

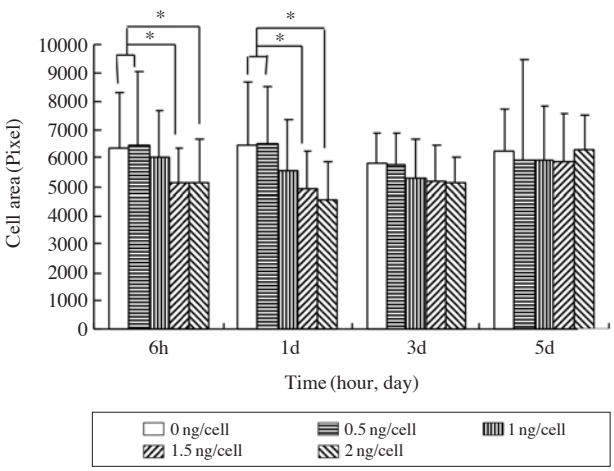


**Figure 2.** Cell size evaluated with Image Pro Plus 6.0 at 0, 0.5, 1, 1.5, 2 ng/cell at 6h, 1d, 3d and 5d. Cell size was evaluated by an "Area" function in Image Pro Plus 6.0 with pixel as the unit. Chondrocytes in other groups were compared to 0 ng/cell group. Before 1d, there was instance of slower spreading under higher densities of magnetic beads (101%-91% at 0.5-1 ng /cell, 78%-76% at 1.5-2 ng/cell). After 3d, most of the cells in all the groups showed no obvious differences in area (99%-88 % at 3d, 101%-95% at 5d). Significant differences between investigated groups were denoted as asterisk ($18 < n < 30$, $P < 0.05$).

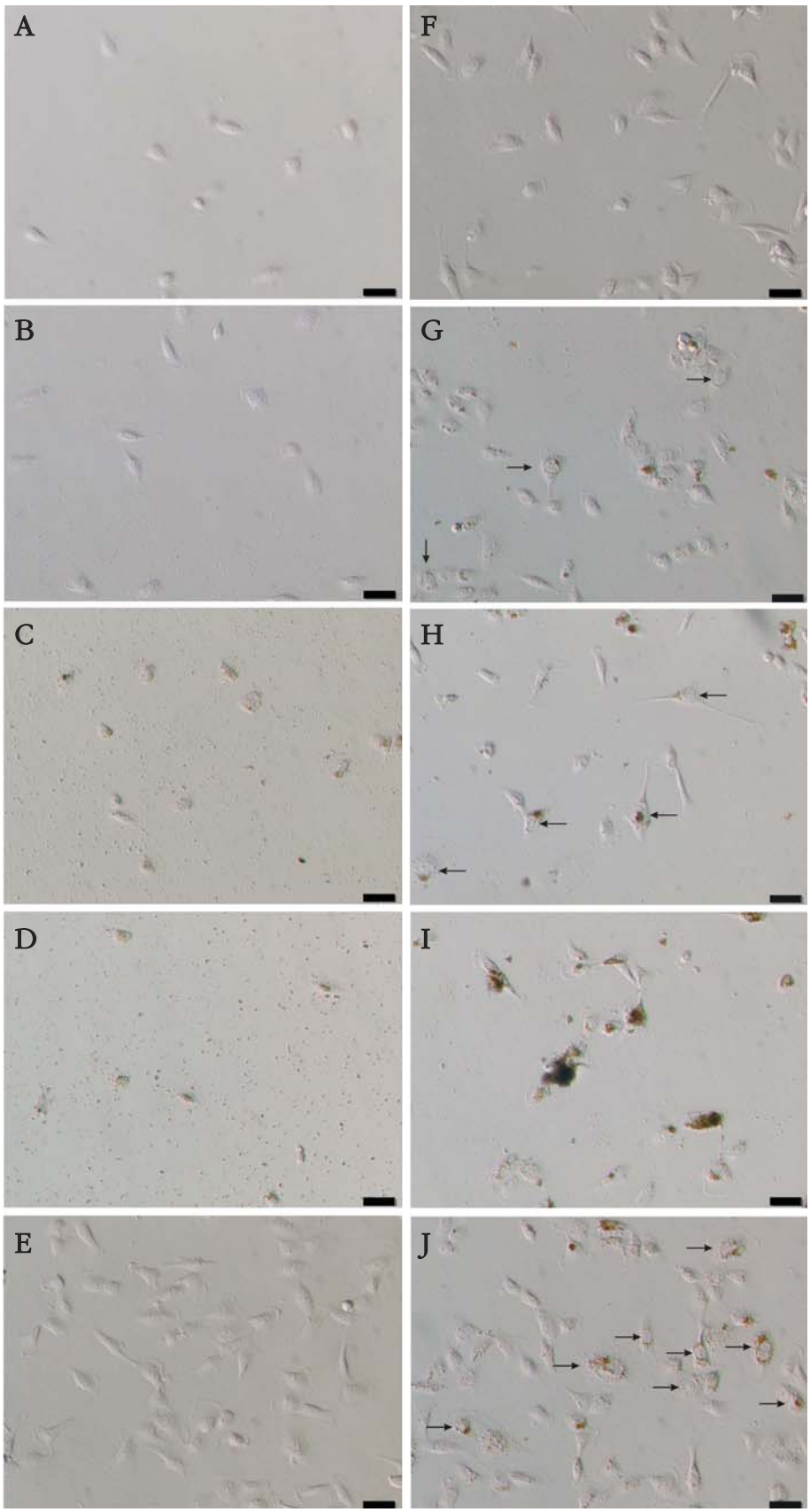


**Figure 3.** Phase contrast microscopic images of cell shape. (A-D) cell images at 0 ng/cell (A), 0.5 ng/cell (B), 1 ng/cell (C) and 2 ng /cell (D) at 6h. Higher concentration group showed smaller cell size. (F-I) cell images at 0 ng/cell (F), 0.5 ng/cell (G), 1 ng/cell (H) and 2 ng/cell (I) at 3d. Most of the cells in all the groups showed no obvious differences in area. (E) 5d image of 0 ng/cell group. (J) 5d image of 1 ng/cell group. The black arrows indicated the magnetic beads tended to gather around the cells and sometimes located around the nucleus. No less than 3 pictures were taken in each group at each time point. Scale bar=50 μm.

**Table 1.** Designed primers for PCR.

| Gene name | Primer sequence (5′ → 3′) | Product length (bp) |
|---|---|---|
| Fibronectin | Forward: CAGACGAGCTTC.CCCAACTGGT<br>Reverse: TGCCTTATGGGGGTGGCCGT | 241 |
| Vimentin | Forward: TGGCCGACGCCATCAACACC<br>Reverse: CTCGACGCGGGCTTTGTCGT | 254 |
| Cyclin D1 | Forward: GTAGCAGCGAGCAGCAGAGT<br>Reverse: CGGTCGTTGAGGAGGTTGG | 218 |
| GAPDH | Forward: ACCCAGAAGACTGTGGATGG<br>Reverse: TTCTAGACGGCAGGTCAGGT | 200 |
| Collagen II | Forward: CCACACTCAAGTCCCTCAAC<br>Reverse: GCTGCTCCACCAGTTCTTC | 247 |
| 18s rRNA | Forward: AAGTACGCACGGCCGGTACA<br>Reverse: AGAGGGGCTGACCGGGTTGG | 193 |

The following gene profile was amplified with PCR: fibronectin (Fn, attachment), vimentin (cytoskeleton[28]), cyclin D1 (CD1, proliferation), glyceraldehyde-3-phosphate dehydrogenase (GAPDH, viability), collagen II (COLII, functional differentiation) and 18s rRNA (internal reference).

were evaluated for a prolonged incubation time. The expression levels of fibronectin (attachment), vimentin (cytoskeleton[28]), cyclin D1 (CD1, proliferation), glyceraldehyde-3-phosphate dehydrogenase (GAPDH, viability), collagen II (COLII, functional differentiation) and 18s rRNA (internal reference) were examined, which reflected the crucial parameters to cell functionality. The acquired results set up a good basis for subsequent experiments, further applications and toxic mechanism studies in cartilage regeneration.

## Cytotoxicity

The results from the MTT assay revealed visible dose- and time-dependent reduction of cell viability between the experimental groups and the negative control (0 ng /cell) (Figure 1). The average percentage of all the experimental groups (0.5-2 ng/cell) to the 0 ng/cell group decreased from 66% to 54% from 6h to 5d. After a sharp drop to 51% at 1d, cell viability remained almost stable thereafter (56% at 3d, 54% at 5d). Initially, the effects of the concentration of the magnetic beads could be disregarded, and the difference between the experimental groups was lower than 20% (74%-55% at 6h, 57%-49% at 1d). As time progressed, especially after 3d, the various concentrations of magnetic beads displayed a more diverse toxicity reaching a 25% difference (69%-44% at 3d, 68%-43% at 5d). The higher the concentration of magnetic beads was employed, the lower the cell viability showed (Figure 1).

In general, chondrocytes exhibited acceptable viability with the polystyrene magnetic beads. However, the cell viability dropped gradually with an increasing concentration of magnetic beads and had a tendency to stabilize as time progressed.

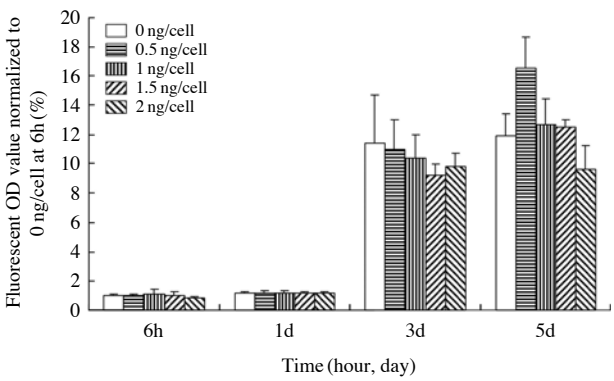


**Figure 4.** DNA quantization with Hoechst 33258 for cell attachment and proliferation. 0-2 ng/cell groups were tested at 6h, 1d, 3d and 5d. Fluorescent OD value was normalized according to the negative control (0 ng/cell at 6h). Before 1d, the similar cell numbers among different groups indicated a non-delay process on attachment. At 3d, although a decline trend of cell number with increasing magnetic bead concentration (97 %-81%, compared to 0 ng/cell at 3d) was observed, no significations showed. At 5d, the other groups, except 2 ng/cell (81 % compared to 0 ng/cell), proliferated faster than the 0 ng/cell group. Low concentrations might hinder cell proliferation at early stages but promote cell division later, while high concentrations of magnetic beads might lead to compromised proliferation as time progresses. Significant variations of tested groups did not occur until 5d and the differences were denoted as asterisk in Table 2 ($P < 0.05$, n=5).

## Cell morphology

Chondrocytes at 0 ng/cell were assumed to be healthy, thus cell area data was normalized to them (Figure 2). The healthy cells attached and extended from roundness to a multi-polar shape within 6h. Before 1d (6h

and 1d), cells in all groups became stretched, but lower concentration groups displayed stretching significantly faster than higher ones (101%-91% at 0.5-1 ng/cell, 78%-76% at 1.5-2 ng/cell). Also, cells at higher concentrations showed less degree of a multi-polar shape than lower ones. After 3d, most of the cells in all groups showed no obvious differences in area (99%-88% at 3d, 101%-95% at 5d) and appeared a normal multi-polar shape (Figure 2 and Figure 3).

The aggregation of magnetic beads could be observed. From 6h to 1d, the magnetic beads accumulated slowly near the cells, which appeared independent of the quantity of the loaded magnetic beads (Figure 3A-D). Furthermore, there was an interesting phenomenon that the magnetic beads gathered around the edge of the nucleus after 3d (Figure 3F-I). This finding was still apparent at 5d, which might indicate an uptake process (Figure 3E, 3J)[6].

In general, most chondrocytes showed healthy morphology; however, there was instance of slower spreading under higher densities of magnetic beads (1.5-2 ng/cell). The magnetic beads tended to gather around the cells and were found sometimes around the nucleus.

**Table 2.** Significant variation of DNA quantification with Hoechst 33258 between two groups at 5d.

| Group | 0 ng/cell | 0.5 ng/cell | 1 ng/cell | 1.5 ng/cell | 2 ng/cell |
|---|---|---|---|---|---|
| 0 ng/cell | | * | | | * |
| 0.5 ng/cell | * | | * | * | * |
| 1 ng/cell | | * | | | * |
| 1.5 ng/cell | | * | | | * |
| 2 ng/cell | * | * | * | * | |

The corresponding histogram was 5d data in figure 4. At 5d, a significant difference of DNA quantification between specific two groups was denoted as asterisk ($P < 0.05$, n=5) in table 2, otherwise no asterisk was recorded. In table 2, the groups in column and row were analyzed in pair.

## Cell attachment and proliferation

At 6h, each experimental group contained a similar cell number normalized to the 0 ng/cell group (~100%) except 88% at 2 ng/cell, which indicated a non-delay process on attachment. However, there were no obvious discrepancies between different concentrations at 6h. As to cell proliferation after 1d, significant variation did not occur until 5d (Figure 4 and Table 2). The

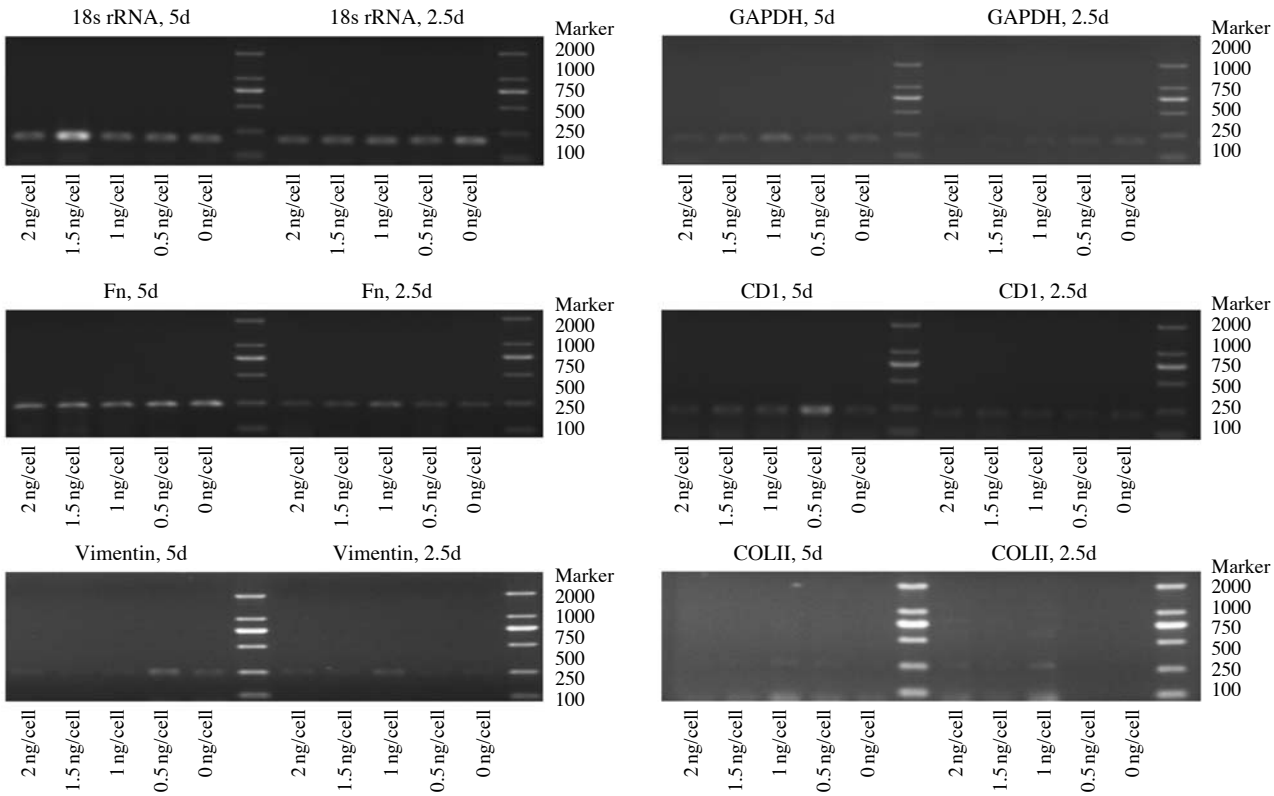


**Figure 5.** Electrophoresis photos of Reverse transcription PCR at 2.5d and 5d. The marker sizes from down to top were 100, 250, 500, 750, 1000 and 2000 bp. Except 750 bp marker band was 150 ng, other bands weighed 50 ng. Semi-quantitation results (1600, Tanon GIS) (n=3) compared to DNA marker (Takara, DL2000) were showed in Figure 6.

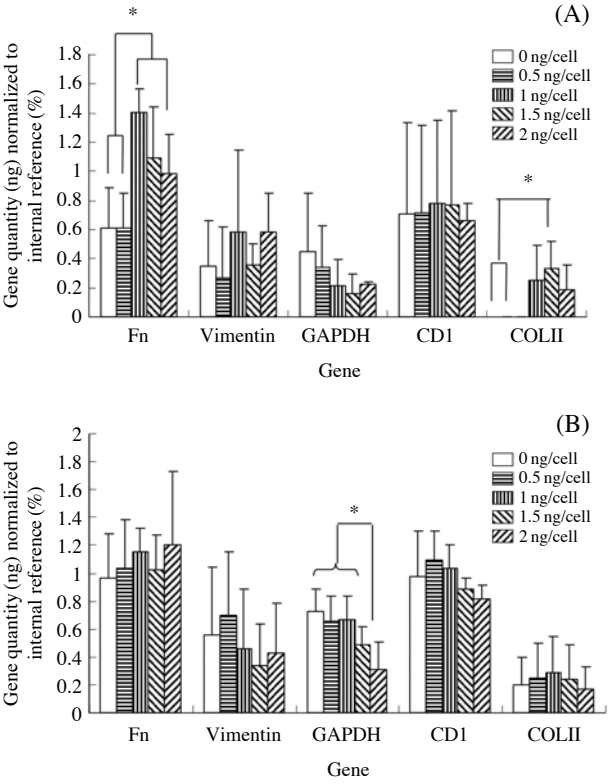


**Figure 6.** Gene semi-quantitation results of chondrocytes blended with magnetic beads. DNA quantitation (ng) was normalized according to the internal reference (18s rRNA) (%). Gene Fn, vimentin, CD1, GAPDH, COLII and 18s rRNA were examined. (A) Distribution of gene profile at 2.5d. A general higher expression of Fn, COLII and vimentin in higher dose loaded groups might indicate a cytoskeleton remodeling correlated with cellular function. GAPDH showed a ladder shaped decline from 0 to 2 ng/cell indicating cell viability. (B) Distribution of gene profile at 5d. Vimentin became lower in higher concentration groups. COLII and Fn levels changed similarly among all groups. Only the lower trend of GAPDH expression in higher dose groups remained the same as 2.5d. Significant variations of tested groups were denoted as asterisk (n=3).

2 ng/cell group only contained 81% cells compared to the negative control at 5d. On the contrary, the other groups except 2 ng/cell, proliferated faster than the 0 ng/cell group, especially the 0.5 ng/cell group exhibiting a cell number of 1.4 times greater than the non-magnetic beads group at 5d (Figure 4).

Exposure to magnetic beads under low concentrations might hinder cell proliferation at early stages but promote cell division later, while high concentrations of magnetic beads might lead to compromised proliferation as time progresses. Moreover, the core-shell magnetic beads showed little detrimental effects on cell attachment.

### Gene expression

The levels of fibronectin (Fn, attachment), vimentin (cytoskeleton), cyclin D1 (CD1, proliferation), glyceraldehyde-3-phosphate dehydrogenase (GAPDH, viability), collagen II (COLII, functional differentiation), and 18s rRNA (internal reference) were examined (Figure 5). At 2.5d (Figure 6A), there was a general higher expression of Fn (61%-62% at 0-0.5 ng/cell, 98%-140% at 1-2 ng/cell), COLII (19%-33% at 1-2 ng /cell) and vimentin (58% at 1 and 2 ng/cell) in higher dose loaded groups, which might indicate a cytoskeleton remodeling correlated with cellular function. Furthermore, GAPDH showed a ladder shaped decline from 0 to 2 ng/cell (45%-22%, except 16% at 1.5 ng/cell), which was in accordance with the MTT assay data. At 5d (Figure 6B), the expression of vimentin and CD1 in higher concentration groups (vimentin, 46%-33%, 1-2 ng/cell) (CD1, 88%-81%, 1.5-2 ng/cell) became minor compared to lower dose ones (vimentin, 56%-70%, 0-0.5 ng/cell) (97%-109%, 0-1 ng/cell). Also, COLII (17%-29%) and Fn (96%-120%) levels changed similarly among all groups. Whereas, the lower trend of GAPDH expression (73%-31%) in higher dose groups remained the same.

As a whole, magnetic beads indeed had effects on the key gene expression of human chondrocytes. These time and dose dependent changes were provided as references for a possible mechanism explanation. Significant variations displayed in Figure 6.

## Discussion

The magnetic beads interacted with cellular membranes in the study. Initially, the insoluble magnetic beads precipitated and formed aggregations due to gravity and electrostatic interaction, respectively[29]. However, magnetic beads were prone to gather on the cells, which could account for an affinity to cellular membranes. Some evidences of this occurrence have been reported, including a preferred bronectin adsorption of magnetic particles (MPs)[1], integrins involved in endocytosis of MPs[30], and transferrin receptor (TfR) responsible for transporting iron into cells[31]. Cells can uptake magnetic beads through three main ways: specific receptor mediated internalization, non-specific phagocytosis and pinocytosis ($<150$ nm) process[1]. The perinuclear magnetic beads were presumed to be a sign of cell uptake[21,32].

Cellular damage caused by magnetic beads can be mainly attributed to the formation of ROS (reactive oxygen species) through the Fenton/Haber-Weiss reactions on mitochondrial membranes: $Fe_3O_4+2H^+\rightarrow \gamma Fe_2O_3+Fe^{2+}+H_2O$ $Fe^{2+}+H_2O_2 \rightarrow Fe^{3+}+{}^{\cdot}OH+$

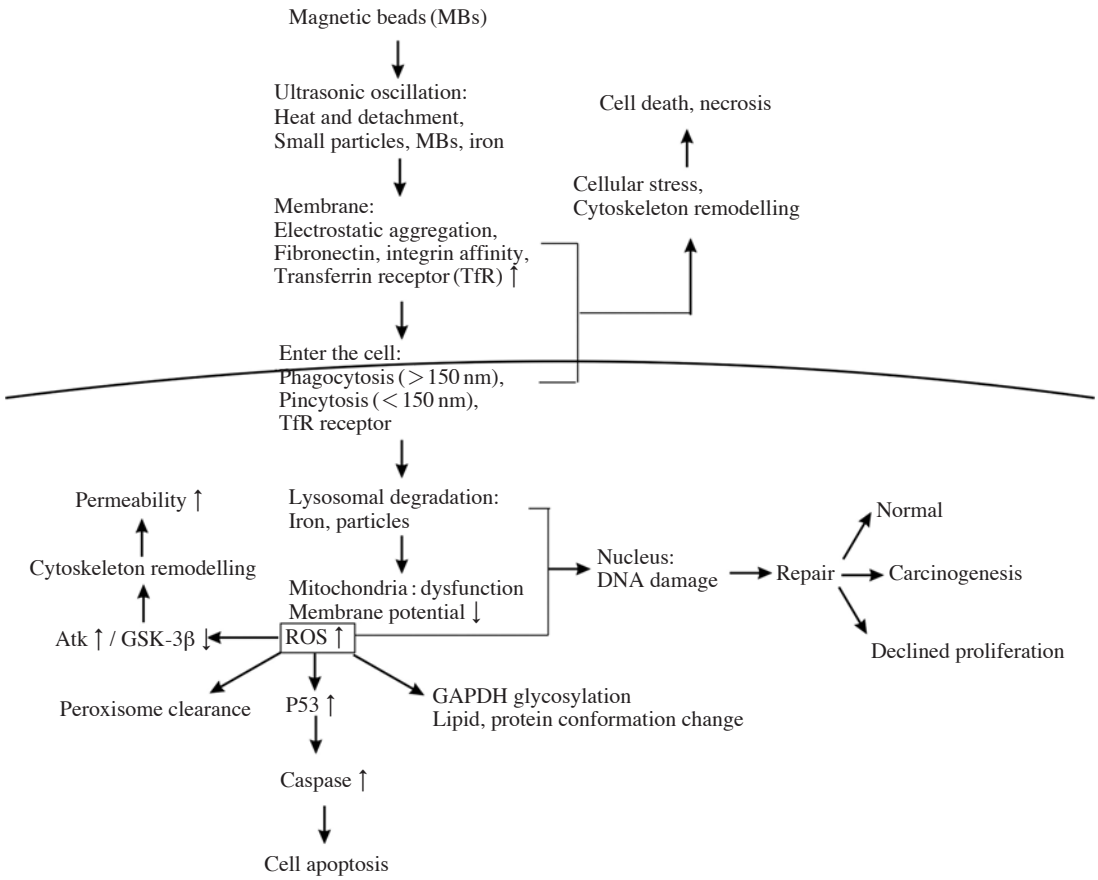


**Figure 7.** Schematic graph describing the possible mechanism of cell behaviors. The side effects were presumed to be related with ROS, iron imbalance, cytoskeleton remodeling, DNA damage, biomolecular adsorption and conformational changes. On the other hand, cells can regulate themselves to compensate for such sudden stimuli, including DNA repair, peroxisome clearance and lysosome enzymolysis. A balanced result presented finally.

$OH^{-2}$. Mitochondria dysfunction can initiate cell apoptosis[33,34]. Imbalanced oxidation/reduction reactions induce the peroxidations of DNA, lipids, proteins and organelles[35,36]. It has been proved that the metabolic enzyme glyceraldehyde-3-phosphate dehydrogenase (GAPDH) in cytoplasm can be denaturized through glycosylation by ROS[37]. The decreased cell viability and GADPH expression corresponded with the aforementioned explanation (Figure 1, Figure 6). DNA peroxidation (8-oxoguanine formation) can be recovered by base excision repair (BER) with delayed cell cycle progression[34]. However, insufficient, inaccurate or excessive repair can lead to DNA lesion, slow division or carcinogenesis[38]. Similar gene levels of cyclin D1 (CD1) and the slow cell proliferation at higher concentrations but fast cell division at lower ones could be seen as a balance of those several described reasons (Figure 4, Figure 6).

There were other mechanisms besides ROS that caused cell damage, including the direct toxicity from magnetic beads and detrimental iron imbalance. (i) The sudden load of magnetic beads may lead to unaffordable cellular stress and even necrosis[21]. Multiple cellular components are inactive or overactive for structural alteration due to adsorption of magnetic beads through electrostatic interactions, hydrophobic interactions, and specific chemical interactions[39,40]. (ii) Iron is a nutrient and regulatory factor for cells. Interruption of the iron homeostasis has broad effects on cytoskeleton structure, proliferation and metabolism[41,42]. Excessive iron resulted in promotion of cyclins and cyclin-dependent kinases (CDKs) through Wnt signaling[43], which was another cause for the cell proliferation findings. (iii) MPs impinging on cells triggers the dynamic remodeling of the cytoskeleton[40]. Since one of the cytoskeleton's main functions is intracellular transport, its alteration has far reaching effects. In our study, the slight poor morphology at higher doses and little effects

on cell attachment were associated with cytoskeleton rearrangement (Figure 2). The gene expression of vimentin showed a higher level early but decreased later at higher doses (Figure 6). This indicated a remodeling process involving uptake, vesicle formation and transportation at early stages, but the processes were regulated to stabilize later.

On the other hand, cells can regulate themselves to compensate for such sudden stimuli. Iron could be consumed by metabolic demands[31]. In addition, the DNA repair mechanism makes efforts to maintain normal gene expression[38]. Peroxisomes are responsible for free radical clearance[38]. Lysosomes can eliminate some deleterious byproducts. Since cell numbers increased over time, the concentrations of magnetic beads were diluted and their effects diminished[40].

As for cellular function, the results showed a promotion at higher doses at 2.5d but a reduction at 5d. Some research revealed human mesenchymal stem cells (hMSCs) with MPs exhibited unaltered viability and proliferation, normal adipogenic and osteogenic differentiation but a marked inhibition of chondrogenesis at 7d. The down-regulation was presumed owing to a specific iron related pathway not affecting viability and proliferation[44]. In contrast, some others reported no effects on chondrogenesis of hMSCs[45]. Our results could be an inhibition of chondrogenesis related to proliferation and viability pathway. At the beginning, collagen II (COLII) gene expression was increased to compensate for a shortage (Figure 6A). However, the inhibition was so strong that the gene level decreased later at higher doses. On the contrary, the lower dose groups had a gradual enhancement as time progressed (Figure 6B).

Previous research failed to reach an agreement about the cytotoxicity of MPs. Both dose-independent[14] and dependent[20] reduction of cell viability was proved. Either decreasing[40] or increasing proliferation[41] was observed. Some studies reported no effects on proliferation or viability[44]. Cells increased in size because of vesicle formation was recognized[22], however cytoskeleton remodeling caused cell size small was also observed[40].

Hence, in the study, a relatively intact study was conducted to human chondrocytes. The core-shell magnetic beads performed cytotoxicity in a dose- and time-dependent way. And the acceptable biocompatible dosage was lower than 1 ng/cell. In addition, considering the insoluble characteristic of MPs, the concentration unit of mass/cell might be more reasonable than mass /mL and mM, which seemed inaccurate after precipitation. Some mechanisms for the cytotoxicity of magnetic beads were concluded in Figure 6.

## Materials and Methods

### Magnetic beads

Bead-shaped superparamagnetic magnetic beads (10 mg/mL, 100-500 nm in diameter) were bought from BaseLine Chromtech (3402). As a core-shell type, each polystyrene ball was wrapped with multiple $Fe_3O_4$ nanoparticles and modified with -COOH. Before being co-cultured with cells, the solution of beads was pulsated for homogeneous distribution by ultrasonic oscillation (KQ218, Kun Shan Ultrasonic Instruments) for 3 minutes.

### Cell culture

Human chondrocyte cell line C28-I2, kindly provided by Mary Goldring at Children's Hospital Boston, USA, were cultured in Dulbecco's modified Eagle's medium (12800-017, high glucose, Gibco) with 10% fetal bovine serum (SV30087.02, Hyclone) and 100 U/mL penicillin-100 μg/mL streptomycin, at 37°C, under 5% $CO_2$. The cells were passaged with 0.25% trypsin (27250-018, Invitrogen) plus 0.02%EDTA (34549, Sigma) at 80% confluence. Magnetic beads were co-cultured with cells at the following concentrations: 0, 0.5, 1, 1.5, 2 ng/cell.

### Cytotoxic test

Cytotoxicity was measured using MTT [3-(4, 5-dimethylthiazol-2-yl)-2, 5-diphenyltetrazolium bromide] assay with 0 ng/cell group as a negative control and latex rubber cut into 0.5 cm∗0.5 cm as a positive control[25]. $3.0 \times 10^3$ cells with magnetic beads in 100 μL of medium were seeded into 96-well culture plates (3599, Costar). Magnetic beads were incubated with cells for 6h, 1, 3 and 5 d respectively. Afterwards, 20 μL MTT (Sigma, 5 mg/mL in PBS solution) was added into each well, incubated for 3 h and removed. 150 μL Dimethyl sulfoxide (DMSO, Merck) was added to dissolve formazan before absorbance was measured at 570 nm with a microplate reader (680, Biorad). Data from the magnetic beads without cells served as the background value. Five replicates were done.

### Cell morphology

Chondrocytes with magnetic beads were seeded at $4.5 \times 10^4$ cells/3 mL medium in 60 mm tissue culture polystyrene (TCPS, 430166, Corning) and were cultured at 37°C in 5% $CO_2$. Cell morphology was recorded by phase contrast microscopy (CKX41, Olympus) at 6h, 1d, 3d and 5d. No less than 3 pictures were taken at each time point. Cell morphology recorded in the photos was evaluated with Image Plus Pro 6.0 software[46].

The selected cell was drawn along its edge to form a closed curve manually. After finishing enough curves, an "Area" function was elected to produce the cell size automatically with pixel as the unit. 18 to 30 replicates were done.

### Cell attachment and proliferation

Cell proliferation was measured through DNA quantization with Hoechst 33258 Dye (H6024, Sigma) at 6h, 1d, 3d and 5d 47. 0 ng/cell group was as a control. Initial cell density was $1.5 \times 10^3$/100 μL in a 96-well plate (3599, Costar) with different concentrations of magnetic beads as indicated previously. After incubation, cells were disrupted in sterilized water and frozen overnight at −20°C. Fluorescence intensity was recorded by a microplate reader (190, Molecular Devices) at excitation and emission wavelengths of 360 and 465 nm, respectively. Five replicates were done.

### Reverse transcription PCR

Cells were seeded at $4.5 \times 10^4$ cells/3 mL medium in 60 mm TCPS. Total RNA was extracted by Trizol Reagent (206101, New Industry) according to the manufacturer's instruction after incubation for 2.5 and 5d. The RNA samples were semi-quantified with Nanodrop (NanoDrop1000, Thermo) to 500 ng. Subsequently, the total RNA was transcribed into cDNA with M-MLV reverse transcriptase (C28025-011, invitrogen) and oligo-dT (FSK-201, Toyobo). PCR (MyCycler™, BioRad) of 30 cycles was performed to amplify the genes. Primers were shown in Table 1. 0 ng/cell group was as a control. Electrophoresis (Beijing Liuyi Instrument Factory) with 1% agarose gel and semi-quantitation (1600, Tanon GIS) (n=3) compared to DNA marker (Takara, DL2000) was performed then[48].

### Statistical analysis

Statistical significances were evaluated with SPSS 13.0 (One-way ANOVA, LSD, $P < 0.05$) and results were expressed as mean ± standard deviation.

**Acknowledgements** The authors would like to thank the support from National Basic Research Program of China (973 Program) (2011CB707500, 2012CB619102) and National Natural Science Foundation of China grant (30970881, 31011140348). And we would like to thank Shamus Moran in Department of biomedical engineering, Georgia Institute of Technology for revising the manuscript.

## References

1. Neuberger, T., Schopf, B., Hofmann, H., Hofmann, M. & von Rechenberg, B. Superparamagnetic nanoparticles for biomedical applications: Possibilities and limitations of a new drug delivery system. *J Magn Magn Mater* **293**:483-496 (2005).
2. Neenu, S., Gareth, J. S. J., Romisa, A. & Shareen, H. D. Potential toxicity of superparamagnetic iron oxide nanoparticles (SPION). *Nano Reviews* **1**:53-58 (2010).
3. Berry, C. C. Progress in functionalization of magnetic nanoparticles for applications in biomedicine. *J Phys D Appl Phys* **42**:1-9 (2009).
4. Hu, S. L. *et al*. In vitro labeling of human umbilical cord mesenchymal stem cells with superparamagnetic iron oxide nanoparticles. *J Cell Biochem* **108**:529-535 (2009).
5. Jin, H. Z. & Kang, K. A. Application of novel metal nanoparticles as optical/thermal agents in optical mammography and hyperthermic treatment for breast cancer. *Oxygen Transport to Tissue Xxviii* **599**:45-52 (2007).
6. Yuge, L. *et al*. Physical stress by magnetic force accelerates differentiation of human osteoblasts. *Biochem Biophys Res Commun* **311**:32-38 (2003).
7. Edwards, B. S., Oprea, T., Prossnitz, E. R. & Sklar, L. A. Flow cytometry for high-throughput, high-content screening. *Curr Opin Chem Biol* **8**:392-398 (2004).
8. Ino, K. *et al*. Cell culture arrays using magnetic force-based cell patterning for dynamic single cell analysis. *Lab on a Chip* **8**:134-142 (2008).
9. Liang, Y. Y., Zhang, L. M., Jiang, W. & Li, W. Embedding magnetic nanoparticles into polysaccharide-based hydrogels for magnetically assisted bioseparation. *Chemphyschem* **8**:2367-2372 (2007).
10. Nan, A. *et al*. Novel magnetic core-shell $Fe_3O_4$ polypyrrole nanoparticles functionalized by peptides or albumin. *Arkivoc*: 185-198 (2010).
11. Bulte, J. W. M. *et al*. Magnetodendrimers allow endosomal magnetic labeling and in vivo tracking of stem cells. *Nat Biotechnol* **19**:1141-1147 (2001).
12. Paulino, A. T. *et al*. One-pot synthesis of a chitosan-based hydrogel as a potential device for magnetic biomaterial. *J Magn Magn Mater* **321**:2636-2642 (2009).
13. Fischer, D., Li, Y. X., Ahlemeyer, B., Krieglstein, J. & Kissel, T. In vitro cytotoxicity testing of polycations: influence of polymer structure on cell viability and hemolysis. *Biomaterials* **24**:1121-1131 (2003).
14. Meenach, S. A., Anderson, A. A., Suthar, M., Anderson, K. W. & Hilt, J. Z. Biocompatibility analysis of magnetic hydrogel nanocomposites based on poly (N-isopropylacrylamide) and iron oxide. *J Biomed Mater Res A* **91A**:903-909 (2009).
15. Berry, C. C., Wells, S., Charles, S. & Curtis, A. S. G. Dextran and albumin derivatised iron oxide nanoparticles: influence on fibroblasts *in vitro*. *Biomaterials* **24**:4551-4557 (2003).
16. Mahmoudi, M., Simchi, A., Milani, A. S. & Stroeve, P. Cell toxicity of superparamagnetic iron oxide nanoparticles. *J Colloid Interface Sci* **336**:510-518 (2009).
17. Mailander, V. & Landfester, K. Interaction of nano-

particles with cells. *Biomacromolecules* **10**:2379-2400 (2009).
18. Bhattacharjee, S. *et al*. Role of surface charge and oxidative stress in cytotoxicity of organic monolayer-coated silicon nanoparticles towards macrophage NR8383 cells. *Part Fibre Toxicol* **7**:25(1)-25(12) (2010).
19. Sohaebuddin, S. K., Thevenot, P. T., Baker, D., Eaton, J. W. & Tang, L. P. Nanomaterial cytotoxicity is composition, size, and cell type dependent. *Part Fibre Toxicol* **7**:22-38 (2010).
20. Ankamwar, B. *et al*. Biocompatibility of $Fe_3O_4$ nanoparticles evaluated by *in vitro* cytotoxicity assays using normal, glia and breast cancer cells. *Nanotechnology* **21**:75102-75110 (2010).
21. Soenen, S. J. H. *et al*. The role of nanoparticle concentration-dependent induction of cellular stress in the internalization of non-toxic cationic magnetoliposomes. *Biomaterials* **30**:6803-6813 (2009).
22. Mahmoudi, M. *et al*. Cytotoxicity and cell cycle effects of bare and poly (vinyl alcohol)-coated iron oxide nanoparticles in mouse fibroblasts. *Adv Eng Mater* **11**: B243-B250 (2009).
23. Zhang, Y., Kohler, N. & Zhang, M. Q. Surface modification of superparamagnetic magnetite nanoparticles and their intracellular uptake. *Biomaterials* **23**:1553-1561 (2002).
24. Karlsson, H. L., Cronholm, P., Gustafsson, J. & Moller, L. Copper oxide nanoparticles are highly toxic: A comparison between metal oxide nanoparticles and carbon nanotubes. *Chem Res Toxicol* **21**:1726-1732 (2008).
25. Hafelli, U. O. *et al*. Cell uptake and in vitro toxicity of magnetic nanoparticles suitable for drug delivery. *Mol Pharmaceut* **6**:1417-1428 (2009).
26. Jeng, H. A. & Swanson, J. Toxicity of metal oxide nanoparticles in mammalian cells. *J Environ Sci Heal A* **41**:2699-2711 (2006).
27. Lin, Z., Willers, C., Xu, J. A. & Zheng, M. H. The chondrocyte: Biology and clinical application. *Tissue Eng*. **12**:1971-1984 (2006).
28. Hyun, J. H., Chen, J., Setton, L. A. & Chilkoti, A. Patterning cells in highly deformable micro structures: Effect of plastic deformation of substrate on cellular phenotype and gene expression. *Biomaterials* **27**:1444-1451 (2006).
29. McCarthy, J. R. & Weissleder, R. Multifunctional magnetic nanoparticles for targeted imaging and therapy. *Adv Drug Deliver Rev* **60**:1241-1251 (2008).
30. von zur Muhlen, C. *et al*. Superparamagnetic iron oxide binding and uptake as imaged by magnetic resonance is mediated by the integrin receptor Mac-1 (CD11b /CD18): Implications on imaging of atherosclerotic plaques. *Atherosclerosis* **193**:102-111 (2007).
31. Thomson, A. M., Rogers, J. T. & Leedman, P. J. Iron-regulatory proteins, iron-responsive elements and ferritin mRNA translation. *Int J Biochem Cell Biol* **31**: 1139-1152 (1999).
32. van der Goot, F. G. & Gruenberg, J. Intra-endosomal membrane traffic. *Trends Cell Biol* **16**:514-521 (2006).
33. Upadhyay, D., Panduri, V., Ghio, A. & Kamp, D. W. Particulate matter induces alveolar epithelial cell DNA damage and apoptosis - Role of free radicals and the mitochondria. *Am J Respir Cell Mol Biol* **29**:180-187 (2003).
34. Soberanes, S. *et al*. p53 mediates particulate matter-induced alveolar epithelial cell mitochondria-regulated apoptosis. *Am J Respir Crit Care Med* **174**:1229-1238 (2006).
35. Stroh, A. *et al*. Iron oxide particles for molecular magnetic resonance imaging cause transient oxidative stress in rat macrophages. *Free Radic Biol Med* **36**:976-984 (2004).
36. Starke, P. E. & Farber, J. L. Ferric iron and superoxide ions are required for the killing of cultured-hepatocytes by hydrogen-peroxide - evidence for the participation of hydroxyl radicals formed by an iron-catalyzed haber-weiss reaction. *J Biol Chem* **260**:99-104 (1985).
37. Zhao, W., Devamanoharan, P. S. & Varma, S. D. Fructose induced deactivation of antioxidant enzymes: Preventive effect of pyruvate. *Free Radic Res* **33**:23-30 (2000).
38. Collins, A. & Harrington, V. Repair of oxidative DNA damage: assessing its contribution to cancer prevention. *Mutagenesis* **17**:489-493 (2002).
39. Lynch, I. & Dawson, K. A. Protein-nanoparticle interactions. *Nano Today* **3**:40-47 (2008).
40. Soenen, S. J. H., Nuytten, N., De Meyer, S.F., De Smedt, S.C. & De Cuyper, M. High intracellular iron oxide nanoparticle concentrations affect cellular cytoskeleton and focal adhesion kinase-mediated signaling. *Small* **6**:832-842 (2010).
41. Huang, D. M. *et al*. The promotion of human mesenchymal stem cell proliferation by superparamagnetic iron oxide nanoparticles. *Biomaterials* **30**:3645-3651 (2009).
42. Berry, C. C., Charles, S., Wells, S., Dalby, M. J. & Curtis, A. S. G. The influence of transferrin stabilised magnetic nanoparticles on human dermal fibroblasts in culture. *Int J Pharm* **269**:211-225 (2004).
43. Chen, Y. C. *et al*. The inhibitory effect of superparamagnetic iron oxide nanoparticle (Ferucarbotran) on osteogenic differentiation and its signaling mechanism in human mesenchymal stem cells. *Toxicol Appl Pharmacol* **245**:272-279 (2010).
44. Kostura, L., Kraitchman, D. L., Mackay, A. M., Pittenger, M. F. & Bulte, J. W. M. Feridex labeling of mesenchymal stem cells inhibits chondrogenesis but not adipogenesis or osteogenesis. *NMR Biomed* **17**:513-517 (2004).
45. Arbab, A. S. *et al*. Efficient magnetic cell labeling with protamine sulfate complexed to ferumoxides for cellu-

lar MRI. *Blood* **104**:1217-1223 (2004).
46. Jung, T. T. K. *et al*. Effects of common topical otic preparations on the morphology of isolated cochlear outer hair cells. *Acta Otolaryngol (Stockh)* **121**:135-139 (2001).
47. Urban, M. R., Fermor, B., Lee, R. B. & Urban, J. P. G. Measurement of DNA in intervertebral disc and other autofluorescent cartilages using the dye Hoechst 33258. *Anal Biochem* **262**:85-88 (1998).
48. Soeth, E. *et al*. Comparative analysis of bone marrow and venous blood isolates from gastrointestinal cancer patients for the detection of disseminated tumor cells using reverse transcription PCR. *Cancer Res* **57**:3106-3110 (1997).